

On the Activation of Integrin α IIb β 3: Outside-in and Inside-out Pathways

Mehrdad Mehrbod*, Stephen Trisno*, Mohammad R. K. Mofrad

Departments of Bioengineering and Mechanical Engineering, University of California, Berkeley,
CA 94720

* These authors contributed equally to this work.

Corresponding Author

Mohammad R. K. Mofrad, PhD

Associate Professor, Department of Bioengineering

University of California Berkeley

208A Stanley Hall #1762

Berkeley, CA 94720-1762

Phone: (510) 643-8165

Fax: (510) 642-5835

Email: mofrad@berkeley.edu

<http://biomechanics.berkeley.edu>

Abstract

Integrin α IIB β 3 is a member of the integrin family of transmembrane proteins that is present on plasma membrane of platelets. Integrin α IIB β 3 is widely known to regulate the process of thrombosis via activation at its cytoplasmic side by talin and interacting with soluble fibrinogen. It is also reported that three groups of interactions restrain integrin family members in the inactive state. These interactions include a set of salt bridges in the cytoplasmic side of the transmembrane domain of integrin α - and β -subunits named as the inner membrane clasp; a hydrophobic packing of a few transmembrane residues on the extracellular side between α - and β -subunits that is known as the outer membrane clasp; and the key interaction group of β A domain (located on the β -subunit head domain) and the β TD (proximal to the plasma membrane on the β -subunit). However, molecular details of this key interaction group as well as events that lead to detachment of β TD and β A domains have remained ambiguous. In this study, we use molecular dynamics models to take a comprehensive outside-in and inside-out approach at exploring how integrin α IIB β 3 is activated. First, we show that talin's interaction with the membrane-proximal (MP) and membrane-distal regions of integrin cytoplasmic-transmembrane domains significantly loosens the inner membrane clasp (IMC) as well as an additional salt-bridge (R734-E1006), which facilitates integrin activation through the separation of integrin's α - and β -subunits. The second part of our study classifies three types of interactions between RGD peptides and extracellular domains of Integrin α IIB β 3. Finally, it is shown that interaction of Arg of the RGD sequence may activate integrin via disrupting the key interaction group between Lys350 on β A domain and Ser673/Ser674 on the β TD.

Keywords

Molecular Dynamics, Simulation, Integrin, Talin, Transmembrane-Cytoplasmic Domains, β TD- β A Domain Detachment.

Introduction

Integrins are a family of ECM-binding proteins that consist of 25 heterodimeric members. Each integrin molecule is composed of an α and a β non-covalently associated subunits. Each integrin subunit consists of a large extracellular domain (ectodomain), a single-pass transmembrane helix, and a short cytoplasmic tail (1-2). Integrins play a host of crucial roles in a variety of cell functions, including linking focal adhesion assemblies to the extracellular microenvironment, facilitating cell migration, transmitting signals bidirectionally, and finally controlling cell growth, differentiation and apoptosis (2-4). Integrin α IIb β 3, which is the major integrin type expressed on the surface of platelets, plays a critical role in platelet aggregation and blood clotting (5-6). Therefore, integrin α IIb β 3 malfunction is marked by several diseases such as thrombosis in myocardial infarction, ischemic stroke, peripheral arterial disease, and Glanzmann thrombasthenia bleeding disorder (6-7). Integrin α IIb β 3 is activated via inside-out and/or outside-in signaling mechanisms, and these two pathways are reported to be discrete while having mutual effects on each other (1-2, 8).

The inside-out activation of integrins is defined as the process of activation that is triggered by a cytoplasmic signal and leads to increased affinity of the integrin head domain for the ligand. Inside-out activation processes modulate integrin α IIb β 3 affinity for extracellular ligands (i.e. fibrinogen) through binding of key cytoplasmic proteins (see Fig. 1). Among various proteins that bind integrins, linking them to the actin cytoskeleton, talin and kindlin are reported to activate integrin via associating with the cytoplasmic tail of integrin β -subunit (4, 9).. The most well known inside-out activation cascade for integrin α IIb β 3 is triggered by binding of cleaved thrombin to proteinase-activated receptor 1 (PAR1) located on plasma membrane of human platelets. This binding leads to phospholipid hydrolysis, which results in the generation of inositol trisphosphate (IP3) and diacylglycerol (DAG), and an increase in cytosolic free Ca^{2+} . The elevated concentrations of Ca^{2+} and DAG, which in turn activates CALDAG-GEF1 and protein kinase C (PKC), converts RAP1 from a GDP-bound to a membrane-attached, GTP-bound form. Activation of RAP1 leads to recruitment of its effector, RAP1-GTP-interacting adaptor molecule (RIAM), and its binding partner, talin 1, to the plasma membrane. This facilitates access of talin to the integrin β 3 tail and talin-induced activation of α IIb β 3 integrin (4). Two major interactions attach transmembrane domains of α - and β -subunits: the Outer Membrane Clasp (OMC) embedded within the lipid bilayer and the Inner Membrane Clasp (IMC) located near the membrane proximal cytoplasmic tail between the integrin subunits (2), once released, the transmembrane-cytoplasmic domains of integrin are separated and activated, causing the extracellular domains to be more receptive to ECM ligand binding. Binding of integrin β 3 subunit to talin-1 is one of major factors that disrupts the interactions between the two integrin subunits, separating the transmembrane-cytoplasmic domains (9). Current study provides molecular-resolution simulations that demonstrate how talin head domain binding to transmembrane-cytoplasmic domain of integrin β 3 subunit mechanically loosens the inner membrane clasp.

On the other hand, the outside-in activation is identified by interactions of integrin extracellular head domain with the ECM ligand or divalent cations that lead to partial unfolding of the extracellular domain and separation of integrin subunits . . Integrin β 3 subunit is known to be

the major regulator of activation for integrin α IIb β 3 and α v β 3 (10-11). Binding of divalent cations with integrin head domain (i.e. β A and β -propeller domains on the extracellular side) is reported to determine the integrin activation state. There exist three divalent metal ion binding sites on Integrin β A domain. The first one, termed as metal ion-dependent adhesion site (MIDAS) is coordinated with Mg^{2+} , while the two other cation binding sites, called adjacent to MIDAS (ADMIDAS) and ligand-induced metal binding site (LIMBS) located on the opposite sides of MIDAS, are coordinated with Ca^{2+} (10, 12-13). High concentrations of Ca^{2+} reinforces the bent, inactive state of integrin α v β 3, while in presence of Mn^{2+} , a cation that activates integrins, most integrin α IIb β 3 molecules, observed by electron microscopy, were in an extended conformation (14). It is proposed by some researchers that the RGD ligand and divalent cation share a common binding pocket on the integrin β 3 head domain on the interface of β A and β -propeller domains (15-16). Importantly, external force has also been shown to directly activate certain types of integrin and prolong their ligand-bound lifetime (17-18). Last but not least, integrin head domain interaction with the ligand at metal-ion dependent binding sites is shown to activate integrins though its details are not fully agreed upon yet. Also, whether an interaction between the CD loop of β TD and β 6- α 7 loop of β A domains regulates integrin activation remains highly controversial (19-20). Hence, we explored potential effects of RGD-binding to integrin α IIb β 3 through positioning two soluble RGD peptides proximal to metal ion-dependent binding sites and one near the β A- β TD domains interface.

Two mechanistic models are widely invoked to describe the behavior of integrins: the switchblade and the dead-bolt model (21). According to the switchblade model, integrins take on three distinct conformations, corresponding to their inactive, active, and ligand-bound states. The inactive state of integrin is featured by a bent-over configuration wherein the molecule shows a low affinity for ECM ligands (see Fig. 1) (21). Also, in inactive state, inner and outer membrane clasps hold the transmembrane domains of integrin together (1). Integrin activation results in a stretched conformation and breakage of the inner and outer membrane clasps, most likely via presence of a competing molecule, e.g. talin and kindlin, that occupies these binding sites on the transmembrane domain of integrin β -subunit (2, 4). Activated integrin is known to have significantly higher affinity for ECM ligands (14). Finally, the ligand-bound state takes place when the integrin head domain engages in interaction with an ECM molecule (e.g. fibronectin and fibrinogen). The ligand-bound conformation differs from the non-bonded active state in the sense that the integrin head domain introduces an opening between the α - and β -subunits when in the ligand-bound state (20, 22). Alternatively, the dead-bolt model suggests a significantly smaller conformational change, wherein a hairpin loop between β -strands C and D of the β 3 tail domain (i.e. the CD loop), located on β -subunit proximal to the plasma membrane, functions as a dead-bolt. Upon release of the CD loop, the integrin molecule is activated, as the bonding between the β TD (proximal to the plasma membrane) and β A domains on the integrin head domain is lost (20, 23-24).

Despite numerous experimental studies conducted to shed light on the elaborate mechanism of integrin α IIb β 3 activation from inside-out as well as outside-in perspectives, the atomistic details of either of these mechanisms have remained ambiguous (4, 8). In this study, we developed molecular dynamics models to probe details of inside-out and outside-in activation of integrin α IIb β 3 via integrin-talin interactions. It has been shown previously that outside-in signaling pathways of integrin α IIb β 3 are spatially distinct from those of inside-out activation in platelets

(8). Hence, this study chose to dissect two of the most established pathways for integrin α IIB β 3 activation in molecular details: Talin binding to the cytoplasmic domain of β 3-subunit to represent the inside-out activation, and RGD binding to the ectodomain to simulate the outside-in activation. First, we estimated the strength of the integrin transmembrane bonds (i.e. inner and outer membrane clasps) and showed that the presence of talin head domain bonded to the cytoplasmic domain of integrin β -subunit markedly loosens the inner membrane clasp such that a lower external force is required to separate the transmembrane α - and β -subunits. We focused our attention to the talin-integrin β 3 interaction as the last step of a major cascade of events that leads to integrin activation to show, in molecular details, the contribution of this critical event in dissociating integrin transmembrane domains. Furthermore, using the full-length crystal structure of integrin including the ectodomain and transmembrane-cytoplasmic domains for the first time, we identified potential binding sites of the soluble RGD ligand to the integrin head domain. Based on these results, three likely mechanisms are proposed for integrin-ligand binding. Finally, we explored the dead-bolt model in atomic details, mapping out three key residues that act as the “dead-bolt”.

Methods

Interactions of RGD Peptides with Full-length Integrin

All molecular dynamics simulations were carried out with the program NAMD (25), using CHARMM27 force field. Integrin α IIB β 3 ectodomain (PDB ID: 3FCS chains A and B (26)) and transmembrane-cytoplasmic domains (PDB ID: 2KNC [46]) were obtained from the Protein Data Bank (PDB) and combined to build the full-length integrin α IIB β 3 structure (except residues 954-959 of α -subunit and 684-690 of β -subunit), assuming covalent bonds between residues Cys959 and Gly955 in the α -subunit and Gly684 and Gly690 in the β -subunit. The integrin structure was embedded in a patch of POPC (1-Palmitoyl-2-oleoyl-sn-glycero-3-phosphocholine) lipid bilayer with dimensions of 152x113Å, using the software VMD (27). In all simulations, lipid chains overlapping with the transmembrane domain were removed afterward. PDB files of three RGD peptides were manually produced and positioned in proximity of the integrin head domain as shown in Fig. 2. The system was solvated afterward in a water box with ionic KCl concentration of 150mM (28).

The temperature and pressure of the system were held constant at 1atm and 310K, using Langevin's piston and Hoover's method (25). The time step was taken as 2fs. The cutoff distance for non-bonded interactions was 1.2nm. For all simulations, particle mesh Ewald (PME) method was used for electrostatic force calculations (25). The cutoff distance for non-bonded interactions was 1.2nm. The hydrogen atom bond length was constrained using SHAKE method. The SHAKE method fixes bond lengths between large atoms and hydrogen atoms, preventing unnecessary calculation of irrelevant interactions (29). The system was minimized, at 2000 steps, and equilibrated 6 times with RGD peptides present and once with no RGD peptide in the system as control, each time for ~13ns.

Integrin – Talin Binding

The crystal structure of the transmembrane and cytoplasmic domains of integrin α IIB β 3 was embedded in a patch of POPC. The first step in our simulations was to induce talin-1 FERM head domain to bind to integrin α IIB β 3, which are known to bind to each other (30-31). Using a molecular graphics software VMD, a model was created with the transmembrane-cytoplasmic regions of integrin α IIB β 3 (PDB 2KNC (32)) embedded in a POPC lipid bilayer (27). Talin-1

FERM head domain (PDB 3IVF (33)) was placed with the F3 (PTB-like) domain, facing the integrin β 3-subunit with a 27Å distance between the center of mass of the F3 domain (L320) to β 3 residue W739. The system was solvated, then neutralized and ionized to a concentration of 150 mM NaCl. The system underwent minimization (2000 steps) and equilibration for 7ns, before each center of mass in the F0-F3 talin domains were given a nudge for 1ns ($k = 0.07\text{kcal/mol/\AA}^2$; velocity = 17.5 Å/ns) in the direction to minimize the mentioned 27 Å distance. Following that, the system was allowed 28ns to equilibrate. At the end of the total 36ns, we nudged the F0-domain of talin for 1ns ($k = 0.06\text{kcal/mol/\AA}^2$, velocity = 12.5 Å/ns) to tilt the F3 domain of talin towards integrin β 3-subunit. This was performed to promote the membrane proximal interactions between F727 and F730 on β 3 subunit to the S1-S2 loop of talin F3 (30). Following that, the system was equilibrated for 9.5ns.

Comparison of IMC Interactions in Integrin versus Integrin-Talin Systems

With the end state of the system from the integrin-talin binding, twelve simulations were run with the following procedure. The final system coordinates were minimized to re-randomize the initial velocities and then equilibrated for 5ns. Next, 5ns steered molecular dynamics (SMD) simulations were run with the following parameters: $k = 0.05\text{kcal/mol/\AA}^2$ and velocity = 10Å/ns. The spring constant and pulling velocity were reduced to allow for potential conformational changes to occur that would affect the necessary force required to maintain the pulling of the dummy atom. The atom being pulled on is the carbon- α of R995 (the α IIB subunit's contribution to the Inner Membrane Clasp, or IMC) and in addition, the other two residues on the β 3 subunit (D723 and E726) of the IMC were fixed (see Fig.S2).

With integrin α IIB β 3 alone, the same steps were taken excluding talin and the steps needed to bind talin to integrin. Twelve simulations were run first to minimize and equilibrate for 5ns, and then those same residues were pulled and fixed for 5ns.

Analysis of Results between Integrin versus Integrin-Talin Systems

For the first step in the binding of integrin-talin, visual inspection and energy plots were used to assess the tightness of the binding. For the comparison of integrin to integrin-talin systems, besides qualitative analysis, three parameters were used to compare those results quantitatively: the force and work required to break the IMC, the distances of the IMC residues prior to the pulling/fixing simulations, and the initial energies of the IMC residues prior to the pulling/fixing simulations.

To calculate the force required to break the IMC, the van der Waal's (VdW), Electrostatic, and total non-bonded (VdW + Electrostatic) energies were calculated between the β 3-subunit subunit residues D723/E726 and the α IIB-subunit residue R995 was calculated throughout the entire simulation. When the energy of interaction is consistently held above -10kcal/mol, the force at that point in time is defined as the force required to break the IMC. The work to separate the IMC was calculated using the scalar projection of the force vector to velocity of the pulled atom (R995 carbon- α), integrated over the time required to separate a particular distance. The initial energy of the IMC prior to the pulling/fixing simulation was also recorded from that data with 100ps window-averaging. The initial distance was also calculated as the average distance between the carbon- α atoms of D723-R995 and E726-R995 from the entire distances of these

atoms throughout the simulation with 100ps window-averaging. In addition, the interaction energies between K320 on talin and D723 on integrin $\beta 3$ were calculated.

Finally, a permutation two-sample t-test was used to check the statistical significance of the differences in those parameters between the two conditions, integrin-talin or integrin alone, with a sample size of 12 values in each condition. A permutation t-test follows a standard unpaired two sample t-test with the equation:

$$t = \frac{\bar{x}_1 - \bar{x}_2}{\sqrt{\frac{s_1^2}{n_1} + \frac{s_2^2}{n_2}}}$$

where \bar{x}_i = mean of the values of the i^{th} condition

s_i = standard deviation of the values of the i^{th} condition

n_i = number of values in the i^{th} condition ($n_1 = n_2 = 12$ in our case),

except that a permutation t-test does not require the assumption of a Gaussian distribution to determine the p-value for significance (34). In our permutation test, we generate the distribution of t-values for every possible condition switch arrangement. Then we test if the actual t-value is greater than 95% of the permuted t-values this distribution for a one-tailed test, or the absolute t-value is greater than 95% of the absolute permuted t-values for a two-tailed test. In this case, we performed a one-tailed test because we hypothesize that our parameters will shift in one direction, which with reference to the integrin-only condition, is towards a lower IMC binding energy (larger distance, less force to separate) for the integrin-talin condition.

Simulation and Analysis of Integrin-talin Interactions Using Full Integrin Structure

Having obtained a full-length integrin $\alpha\text{IIb}\beta 3$ structure, we placed it inside a membrane, solvated and ionized it with 150mM NaCl, and ran a minimization and equilibration simulation for 6ns. Next, with our equilibrated the full-length integrin structure, a similar model consisting of integrin and talin-1 FERM head domain was built, with a similar orientation and initial distance maintained between integrin $\beta 3$ -subunit and F3 domain of talin-1. This model was minimized and equilibrated for 4ns, ten times to get a random sample of velocities and trajectories. From the simulations, we measured the final distance (at 4ns) between R734-E1006, between αIIb and $\beta 3$ extracellular domains, between βTD and βA domains, and between the center of masses of selected regions of $\beta 3$ -subunit integrin and talin-1 F3 domain. Finally, the Spearman's tests of dependence were performed to further pinpoint which region of $\beta 3$ -subunit tail is correlated to the weakening of this additional interaction and whether the degree of talin binding to the integrin $\beta 3$ -subunit affected integrin's extracellular conformation.

Results

Interactions between the soluble RGD and integrin potentially activates integrin $\alpha\text{IIb}\beta 3$

In order to probe likely binding sites of the soluble ligand, RGD sequences were placed at three locations proximal to the integrin head domain previously reported as potential binding spots of integrin for fibrinogen (10, 13, 20). Depicted in Fig. 2 are locations of the three soluble RGD ligands relative to the integrin molecule. Two RGD peptides were positioned in vicinity of the interface between β -propeller domain of α -subunit and βA domain of β -subunit, while another RGD peptide was located in proximity of the pocket formed by βA and βTD domains of β -subunit. Fibrinogen is a large macromolecule with a low transformational as well as rotational

diffusion coefficient (35). Therefore, identifying the potential binding sites of the fibrinogen on the integrin head domain requires an excessive amount of computational time, i.e. several seconds or even longer, which is beyond the time scale of current molecular dynamics models. Hence, merely a functional part of the fibrinogen molecule, i.e. the RGD sequence, was located close to the integrin head domain and allowed to diffuse freely.

The integrin molecule embedded in the lipid bilayer was solvated in a water box, minimized in 2000 steps of 2fs, and equilibrated for at least ~ 13 ns. The three RGD peptides diffused throughout the water box, until they formed interactions at various regions on the integrin head domain. The simulation was repeated seven times, corresponding to a total of ~ 104 ns. RGD peptide 3 (see Fig. 3) interacted with various binding sites located on the integrin head domain and/or within the inner pocket formed by the bent molecule. However, RGD peptide 1 and 2 together interacted with a fewer number of binding sites on the interface of βA and βTD domains. Intriguingly, RGD3 was confined to the βA and βTD pocket in all simulations, whereas RGD1 and RGD2 remained associated with the head domain only in half of the simulations. Interactive residues on each subunit are shown in table 1.

Interactions that lasted for a minimum of ~ 3 ns after their initial formation were called “permanent bonds” as opposed to those that formed only intermittently, termed “temporary bonds” hereinafter. Depicted in Fig. 3 are the distance between interacting residues of integrin within βA - βTD and RGD3. It is noteworthy that interactions between the RGD peptide and extracellular domain of integrin are mainly salt bridges, as the RGD peptide is equipped with a strong basic and an acidic residue (i.e. Asp and Arg) with long side chains at its two ends that are separated by a small hydrophobic spacer (i.e. Gly). Thus, all permanent bonds shown in Fig. 3 are of $\sim 4.5\text{\AA}$ bond length, which is the characteristic length of a salt bridge (34, 36).

According to the nature of bonds in the simulated trajectories, integrin-RGD bindings were classified into three major groups; the first group (i.e. type1 bond) comprised interactions with only a single, permanent interaction between the RGD peptide and integrin, as demonstrated in Fig. 3a and 3b. Permanent bonds formed as a result of type1 bonds with minimal fluctuations in all cases. Fig. 3a presents the bond distance between Arg of RGD3 and Asp817 on Calf2 domain of α -subunit, whereas Fig. 3b shows the bond distance between Arg of RGD3 and Asp127 on βA domain of β -subunit.

The second type of binding that occurred in two of our simulations included bindings in which one side of the soluble RGD peptide interacted permanently with βA domain on the integrin head domain, while the other end only showed temporary engagement with membrane proximal domains of integrin. In one simulation, the Arg side of the soluble RGD formed a permanent bond with Glu312 on βA domain (see Fig. 3c). This interaction served as an anchorage for the ligand, while the other side interacted temporarily with Lys650 on the βTD . Another permanent interaction formed between Arg of RGD3 and Asp232 of β -propeller domain of the αIIb subunit, whereas the Asp side of RGD3 formed a temporary interaction with Asn313 on βA domain (see Fig. 3d).

The other, and the most complex, type of interactions involved one permanent binding site and two temporary interactions on the integrin molecule that competed with each other. This group

of interactions featured one end of the free RGD peptide tethering to the β -subunit permanently, while other short-term bindings also taking place with the other end of the RGD peptide. For instance, Fig.3 e shows a permanent bond between Arg of RGD3 and Asp628 on Calfl domain of α -subunit (blue) as well as temporary bonds between Asp of RGD3 with Arg897 on Calfl domain of α -subunit (green), and Lys600 on the linker region between EGF-1 and β TD (red). Although partial detachments were seen in a few of the simulations, a full separation of β TD and β A domains was only observed in one out of six RGD-included simulations, when RGD3 interacted with three binding sites as depicted in Fig. 3f. A permanent, polar interaction (shown in blue in Fig. 3f) was formed between Arg of RGD3 with Glu671 on the β TD. Importantly, it was observed that the electrostatic interactions of Ser673 and Ser674 on the β TD with Lys350 serve as a key for activation of integrin α IIb β 3, as depicted by Fig. 4. This simulation was run for \sim 21ns. The key residues on the β TD (i.e. Ser673 and Ser674) continued to interact with Lys350 until $t=7.5$ ns (see Fig. 4c). However, as Arg of the RGD peptide reached the vicinity of Ser674 at $t=7.5$ ns, Arg of the RGD peptide competed with Lys350 for Ser674 and the key interaction was highly disturbed (Fig. 4d). Finally, the key interaction was fully removed as Asp of the RGD peptide engaged in a competitive interaction with Lys600 and Lys611, pulling the β TD away from β A domain (Fig. 4e). As a result of the RGD peptide replacing Lys350 on β A domain, the β TD swung open, separating from β A domain (see Fig. 4a and 4b). The open conformation of the β TD appeared to be stable insofar as the β TD remained open for another 4.5ns until the end of the simulation, as shown in Fig. S1. Finally, we repeated the simulation one more time without any RGD peptides included. As expected, β TD and β A domains remained attached in the absence of RGD.

We observed that the dissociation of β TD and β A domains caused the β TD to snap back, which induced a slight rotation in the β -subunit transmembrane domain (about 3° over the course of our simulations) in a lever-like motion. This rotation increased the angle between the α - and β -subunit transmembrane domains. We conducted energy analyses to measure the electrostatic energy between the α - and β -subunit transmembrane domains for the case where there was no RGD peptide as well as the case where the integrin activation was observed. Interestingly, the electrostatic energy of interaction appeared to dramatically decrease after the β TD and β A domains separated (see Fig. 5a). A tiny rotation of the long, β -subunit transmembrane domain increased the distance between acidic and basic residues on α - and β -subunit transmembrane domains that considerably weakened the inner membrane clasp.

Integrin – Talin Binding

To study the effect of talin on integrin activation, we first needed to create two separate conditions: the experimental condition, integrin with talin bound, and the control, integrin alone. To create our experimental condition, we promoted the binding of talin to integrin through a series of equilibration and steering simulations. After the 48ns of equilibration and nudging, we observed binding between integrin and talin. Our results match that of the suggested mode of binding in literature (2).

First, hydrophobic packing is evident between conserved residues and motifs, W739 and NPLY (744 to 747), on integrin β 3, and residues on F3 domain of talin. The identified residues on F3 domain of talin that bind to W739 on integrin β 3-subunit are the residues R358 and A360 on the S5 β -sheet on talin, which form a pocket for W739 (37). Additionally, the NPLY motif interacts

with these S5 residues and additional residues, A389, Q390, A393, and I398, on the final H1 helix of the F3 domain (Fig. 6). Finally, after the nudges to tilt talin, one (F727) of the expected two residues on β 3-subunit, F727 and F730, embedded itself in talin S1-S2 loop region strand, consisting partly of residues K318, M319, and K320 (30).

Effect of Talin binding to Integrin

Using the integrin-talin and integrin-alone models, we randomized the initial velocities in 12 repetitions, equilibrated for 5ns, and pulled apart the IMC for 5ns. From these simulations, we were able to identify significant differences in the following parameters. The Inner Membrane Clasp (IMC) of integrin had a change in conformation with the binding of talin. This is evident with the three parameters used to quantify the state of the IMC. The average distance between the carbon- α atoms of D723 – R995 and E726 – R995 shows that talin induces a bulge in the IMC even prior to the steered separation. The mean distances, as indicated by distance “d” in Fig. S2, for both the integrin-talin and integrin alone conditions were 9.8Å and 13.5Å, respectively, and this difference was significant using a permuted two-sample, one-tailed, t-test ($p < 0.0003$). As a result of this increase in distance, the interaction energy between the acidic β 3 and basic α IIB IMC residues was also diminished (corresponding to less negative energy, see Fig. 7a and 7b). The mean nonbonding energy for the integrin-talin systems was -93.4kcal/mol and for the integrin-only system was -133.4kcal/mol (Fig. 7), and again this difference is significant ($p < 0.002$). More interestingly, in all 12 simulations, the interaction energy between the IMC residues was never stronger than -129.7kcal/mol in integrin-talin simulations, whereas the strongest observed energy was -163.6kcal/mol in integrin-only simulations.

The last parameter investigated was the force required to break apart the IMC. As expected, with talin bound to integrin, the force required to break the IMC was lower than without talin. The mean force required, given the spring constant of $k = 0.05\text{kcal/mol/\AA}^2$ and constant-pulling velocity 10\AA/ns of the carbon- α atom of R995 while fixing the carbon- α atoms of D723/E726, was $224.6 \pm 9.75\text{pN}$ with talin bound and $249.8 \pm 12.2\text{pN}$ with integrin only (mean \pm standard error). This difference was slightly significant ($p < 0.04$). These differences in initial energies, distances, and forces between the integrin-talin and integrin-alone conditions were confirmed with the difference in work of approximately 1000kcal/mol required to separate the IMC, up to 16\AA of separation (Fig. 7c). In addition, with the integrin-talin simulations, a basic residue, K320, on talin’s S1-S2 loop interacted with the integrin β 3 IMC residue D723 before and after the breakage of the IMC, with interaction energies of -75.2kcal/mol and -84.5kcal/mol, respectively.

One interesting difference between the integrin-talin versus the integrin-only system is that there is an additional salt bridge interaction between R734 on β 3 and E1006 on α IIB-subunits with the integrin-talin systems (Fig. 7). Quantitatively, we observed that in the distance between the most terminal carbons on R734 and E1006 was significantly different between the integrin-talin (5.25 Å) and the integrin only (16.1 Å) conditions, with $p < 0.0003$.

Effect of Talin binding to Full Integrin Structure

Using the full-length integrin structure, we assessed the effects of the F3 domain of talin binding to specific local regions on the integrin β 3-cytoplasmic tail. Focusing on this new interaction, R734-E1006, we found an overall negative correlation between the center of mass distances of

integrin $\beta 3$ -cytoplasmic tail to talin F3 domain and the energy of interaction and distance between R734 and E1006. In other words, as talin F3 domain approaches integrin tail, the distance between R734 and E1006 enlarges, which also results in a weakened interaction energy. However, between the two independent measures, energy of interaction is more reliable than distance in producing significant results. Upon closer analysis (see Table 2), a stronger correlation is observed when selecting the dependent variable as the center of mass of a subdomain of cytoplasmic $\beta 3$ -subunit, specifically the region from the NPLY motif onwards (termed NPLY-T762), to measure the distance to the center of mass of the F3 domain of talin ($\rho = -0.82$, $p = 0.0038$). This suggests a greater significance in the membrane-distal binding of $\beta 3$ -integrin to F3 domain of talin-1. Similarly, we also examined the potential conformational changes in the integrin extracellular domain followed by the F3 domain of talin binding to integrin $\beta 3$ -cytoplasmic tail. In the two relevant parameters of conformational changes to the integrin extracellular domain, which are the centers of mass distances between the α IIB and $\beta 3$ extracellular domains and between β TD and β A domains, the degree of talin binding did not show any significant effects to alter integrin extracellular conformation (table 3).

Discussion

Although integrin has been a subject of intensive study over the past two decades, molecular details of its function have remained ambiguous (3, 20-21). [23,24,25] As shown in Fig. 1, interaction of thrombin proteinase-activated receptor 1 (PAR1) with thrombin triggers the integrin α IIB $\beta 3$ activation pathway, which finally leads to thrombosis (1, 4, 38). Therefore, understanding how integrin α IIB $\beta 3$ functions paves the road for deciphering pathways that regulate thrombosis (38-39). Here, we performed a series of molecular dynamics simulations to observe how exposing integrin α IIB $\beta 3$ to soluble RGD peptides as well as talin head domain may affect the integrin structure. Integrin α IIB $\beta 3$ is a highly studied member of the integrin family, which is present in platelets, enabling them to interact with soluble fibrinogen (a specialized ligand of integrin α IIB $\beta 3$ that exists abundantly in blood stream). It is widely known that soluble fibrinogen binds the head domain of integrin α IIB $\beta 3$, initiating the blood clotting process by forming a network of fibrinogen ligands with platelets trapped inside it (39-41).

Approaching integrin α IIB $\beta 3$ from the intracellular perspective, we have uncovered new biomolecular, mechanistic details on the inside-out activation process by talin. Although it is known that talin is required for inside-out activation of integrin, the specific mechanism of how integrin is activated through talin is uncertain (42). The current working model suggests that talin binding to the cytoplasmic tail of $\beta 3$ subunit would occur firstly at the membrane-distal region, which then promotes a membrane-proximal (MP) interaction to take place between talin and integrin $\beta 3$ -subunit. This MP interaction is where the mechanism of activation arises (43). What our data suggests is a similar mechanism, in that $\beta 3$ -subunit F727 embedding in talin S1-S2 loop may help allow the IMC salt bridge to loosen its grip because this allows the basic K320 residue to energetically compensate for the IMC salt bridge loss. Furthermore, in the timescale of our simulations, we did not observe the full separation nor significant conformational changes in integrin extracellular domains, which would indicate integrin activation, though previous work suggested that breakage of the IMC salt-bridge by talin is necessary but not sufficient to fully activate integrin (43).

Additionally, we observed a salt-bridge interaction between the most membrane distal regions of α IIB and β 3 integrin subunits with the residues E1006 and R734, respectively. Interestingly, this interaction appeared in two of the four separate simulation conditions, forming in the integrin-talin bound simulations using only the cytoplasmic-transmembrane domains of integrin, and in the integrin-alone simulations using the full-length integrin α IIB β 3. We propose that, one, this interaction may be an artifact of using only the cytoplasmic-transmembrane domains of integrin, and two, the default presence of this interaction using full-length integrin suggests that talin plays an even more important role in integrin activation. Firstly, this artifact in the cytoplasmic-transmembrane simulations may cause the force and work required to separate the IMC under the integrin-talin conditions to be overestimated, and without this interaction, the integrin-talin conditions may be even more favorable towards IMC separation and integrin activation. Secondly and more interestingly, it seems that the membrane-distal interactions of talin and integrin are important for more than solely providing an anchor for the MP interactions to weaken the IMC (43). Instead, we propose that the binding of talin to the membrane-distal region of β 3-subunit cytoplasmic tail weakens this salt bridge E1006-R734 interaction, which is the first step in integrin inside-out activation.

Integrin is also activated via association with an extracellular ligand, a process called outside-in activation. It is reported that integrin α IIB β 3 has a high affinity for the RGD sequence of fibrinogen (3, 6, 44). Interactions between integrin α IIB β 3 and fibrinogen are reported to occur on the interface of β -propeller domain of α IIB and β A of β 3. Particularly, RGD peptides are shown to associate with a region of β 3 defined by Asp109 and Glu171 as well as another region limited to Ser211 and Gly222 (15-16). Nonetheless, a number of studies showed that integrin α IIB β 3 head domain interacts solely with a C-terminal region of the fibrinogen (i.e. γ C) rather than the RGD sequences on fibrinogen α -subunit (10, 13). To address this controversy making best use of the computational time, instead of modeling the entire fibrinogen molecule, we placed two RGD sequences at regions of integrin α IIB β 3 head domain that had been reported to have high affinity for fibrinogen (3, 10). An RGD peptide was positioned in vicinity of β TD- β A domain interface, another sensitive region that is suggested to contribute to integrin activation, to explore its potential interactions especially ones that could regulate integrin function. The small size of RGD peptides conferred them high diffusivity and capability to sweep the space in proximity of the sensitive areas of integrin α IIB β 3. We initiated our simulations with inactive integrin α IIB β 3, wherein β A domain of the integrin head domain is attached to the membrane-proximal β TD. This forms a pocket-like configuration between the integrin head domain and membrane-proximal region, which is geometrically appropriate for the long, coiled-coil molecule of fibrinogen to insert into. Because the RGD motif of fibrinogen is located on the surface of γ -subunit of fibrinogen, it has high potency for detecting RGD-sensitive regions of integrin α IIB β 3

The association constant for the integrin-peptide interaction is:

$$k_a = \frac{[IP]}{[I][P]}, \quad (1)$$

where [IP], [I], and [P] are concentrations of integrin, free RGD peptide, and integrin-RGD complex, respectively. The association constant is related to the free energy of association as follows:

$$(2) \quad k_a = e^{\frac{-\Delta G}{k_B T}},$$

where ΔG , k_B , and T are the free energy of association per mol, Boltzmann constant, and temperature, respectively. Our simulations indicated that for the highly dynamic RGD binding sites in the β TD- β A pocket, 10ns is a reasonable time scale for bonds to form and break down at least once (see Fig. 3). As the free energy per mol of a significant electrostatic bond in amino acid is typically taken as 5 kCal/mol (45-46), substituting that value for ΔG in Eq. 2 and solving at $T=310K$ yields $k_a \sim 0.06 \text{mol}^{-1}$. According to the ergodic hypothesis in statistical thermodynamics, for a stochastic system any average of thermodynamic parameters over the entire volume of the system at any instant in time equals the average of the same parameter taken over a long time span at a single point in the system (47). Hence, as a first approximation, we can assume the free concentrations of integrin and peptide (denoted as [I] and [P]) are proportional to the sum of time spans that the system experiences the unbound state. On the other hand, the concentration of the complex (denoted by [IP]) is proportional to the accumulative time period that the system spends in the unbound state. Therefore, the minimum association constant for significant bond formations ($k_a=0.06 \text{mol}^{-1}$) is corresponding to a binding time of at least 3ns within a simulation scale of 10ns. We defined bindings that remained associated for more than $\sim 3\text{ns}$ as permanent bonds and bindings with life spans any shorter than 3ns as temporary bonds.

Our simulations highlighted several binding sites for the RGD peptide on integrin α IIB β 3, most of which were either inside or proximal to β A- β TD pocket. Binding sites of integrin α IIB β 3 for RGD peptides in this region fell into three distinct categories, wherein permanent interactions always form at the Arg end of the RGD peptide. This could be attributed to the highly basic side chain of Arg that facilitates formation of permanent salt bridges. The first category of bonds formed between Arg of the RGD peptide and integrin. Although this group included permanent bindings, these bindings did not contribute to detachment of β A and β TD domains within our simulation time because they were not able to disturb the key interaction (i.e. Lys350 with Ser673 and Ser674). In the second type of interactions, Arg of the RGD peptide formed a permanent bond with integrin α IIB β 3, and Asp of the RGD peptide formed a temporary bond, which was highly fluctuating and unstable. Finally, the third and most complex type of RGD peptide-integrin interactions were composed of a permanent interaction of Arg of the RGD peptide with integrin α IIB β 3 at one end and a competitive, temporary interaction of two other residues with Asp of the RGD peptide at the other end. Within the time scale of our simulations ($\sim 13\text{ns}$), one out of two observed, type3 interactions fully detached β A and β TD domains, which according to both switchblade and dead-bolt models is equivalent to integrin activation.

After about 7.5ns of equilibration and free diffusion of the RGD peptide in vicinity of the β A- β TD pocket, as depicted in Fig.4, the key β A- β TD domain interactions (i.e. Lys346 with Ser663 and Ser664) were disrupted as a result of the side chain of RGD Arg taking over the OH-group on the side chain of Ser663. About 1ns after the key interaction was disrupted, the β TD swung open and the conformational change continued as Asp of the RGD peptide was engaged in two

competing interactions with Lys590 on the EGF3-EGF4 domain linker region and Lys601 on EGF4 domain of $\beta 3$ -subunit (see Fig.4e). These competing interactions shifted the RGD peptide more toward EGF3 and EGF4 domains, which furthered the distance between βA and βTD domains. It is worthwhile mentioning that since Ser residues do not have significant avidity for Lys, two Ser residues together still do not hold Lys346 on βA domain in a permanent salt bridge (i.e. a bond distance of $\sim 4\text{\AA}$). Hence, this rather weak interaction combined with strong basic identity of Arg side chains may explain how integrin $\alpha IIb\beta 3$ is activated by a soluble, RGD-containing ligand (i.e. fibrinogen).

It has been shown that fibrinogen binds an extensive interface between βA and β -propeller domains of integrin $\alpha IIb\beta 3$ head domain proximal to the metal-ion dependent sites (i.e. MIDAS and ADMIDAS), which leads to integrin activation (10, 13, 48). Aligned with previous studies, RGD1 and RGD2 interacted with the crevice region between βA and βA -propeller on the head domain (15-16). However, we did not observe any significant conformational changes induced in integrin as a result of RGD binding to the head domain. This is aligned with a more recent study that showed functional associations of fibrinogen with integrin occur at RGD-lacking γC peptide of fibrinogen (13). Our study shed light on another important binding site for the RGD motif inside βA - βTD pocket that activates integrin. Our simulations indicated that the pocket formed by βTD and βA domains of integrin is home to several binding spots for the RGD peptide. Short-term interactions between these binding spots and the RGD peptide increase the residence time of the soluble RGD peptide near the pocket, which escalates odds of an interaction occurring between the RGD peptide and the key bonds between βTD and βA domains (i.e. Lys350 with Ser673 and Ser674), which leads to integrin activation via disrupting the key interactions.

Two major mechanisms are reported to “unlock” the integrin inhibitory interactions. While the switchblade model proposes a drastic conformational change, from bent conformation to fully-stretched conformation upon activation, the dead-bolt model suggests more local conformational changes in the molecule due to dissociation of βTD and βA domains [13,23,34,42] The switchblade model suggests that the interaction of the integrin cytoplasmic domain with particular focal adhesion proteins leads to a 135° rotation of the integrin head piece relative to the tail piece. This rotation causes the βA - β -propeller interface to face away from the plasma membrane, thereby becoming available to interact with the ligand (8, 14). The switchblade model is corroborated for different members of integrin family by a number of previous studies. First, when recombinant integrin $\alpha 5\beta 1$ was artificially constrained with disulfide bonds in a bent conformation they did not associate with immobilized ligands (49). For integrin $\alpha v\beta 3$ a double mutation that held the head domain against the leg domains via a cysteine bridge hindered activation (14). In addition, a significant increase in the protein Stokes radius has been recorded for cases where integrins were exposed to RGDFV peptides or Mn^{2+} (i.e. integrin activators) versus the case they are in Ca^{2+} buffer, which is an activation inhibitor (14). However, integrin $\alpha IIb\beta 3$ activation paradigm appears to remain controversial. As detailed monoclonal antibody epitope maps for inactive and active integrin $\alpha IIb\beta 3$ *in vivo* demonstrated similar compact forms consistent with the bent conformation (20, 50). Furthermore, binding of different ligand mimics to integrin $\alpha IIb\beta 3$ in intact platelets has shown distinct conformational changes in the receptor (51).

Another mechanistic explanation for integrin activation was given by the deadbolt model. The deadbolt model assumes that the elongated CD loop of the βTD locks βA domain via forming

bonds with it in the inactive state of the native structure, although the atomistic details of these interactions are not currently clear (20). It is important to note that the deadbolt model does not necessarily exclude a subsequent ligand-induced switchblade swing-out. Interestingly enough, our simulations demonstrated that a disruption in the interactions between β TD and β A domains could be a trigger for integrin activation, recognizing electrostatic interactions of Lys350 on β A with Ser673 and Ser674 on the β TD as a potential regulatory lock.

We observed that the dissociation of β TD and β A domains was succeeded by the β TD snap-back, which caused the β -subunit transmembrane domain to slightly rotate (about 3°) in a lever-like motion. This increase in the angle between the α - and β -subunit transmembrane domains is also reported by previous electron microscopy and biochemical data as a potential activating mechanism for integrin α IIb β 3 (16, 42, 44, 52). However, another model is proposed for a number of other integrin family members (e.g. α 5 β 1) that suggests the hinge region for the scissors-like motion of integrin, upon activation, is located on the interface of α - and β -subunit head domains (49). We measured the electrostatic energy between the α - and β -subunit transmembrane domains for the simulation with no RGD peptides and compared it to the one in which the integrin activation had been observed. Intriguingly, the electrostatic energy of interaction appeared to decrease dramatically after the β TD and β A domains separated. A slight rotation of the long, β -subunit transmembrane domain could considerably increase the distance between charged residues on α - and β -subunit transmembrane domains, which would weaken the inner membrane clasp (IMC). Therefore, we believe RGD interaction with the β TD could be a potential trigger for a complete separation between the transmembrane domains. Although this set of data proposes a key interaction that might function as a regulating “dead-bolt,” the loosening of the transmembrane domain clasps as a result of β TD- β A domain separation suggests subsequent, more drastic conformational changes, and explains how ligand-binding could lead to transmembrane domain separation as proposed by the switchblade model. On the other hand, within the time scale of our simulations, we did not observe any significant conformational changes in the ectodomain nor decreases in β A- β TD interaction energy upon talin binding with β 3 cytoplasmic tail. This suggests that outside-in activation via RGD association with the key residues embedded in β A- β TD pocket occurs more rapidly than inside-out activation followed by talin binding. It is also noteworthy that different activation mechanisms and conformational changes might be at work for various combinations of integrin-ligand interactions.

Conclusion

The activated state of integrin is commonly characterized by three major dissociations: breaking of IMC and OMC, and detachment of β A and β D domains (1, 4, 20, 53). This study attempted to explain the integrin α IIb β 3 function, via exploring how these key interaction groups are disrupted in specific pathways. Our observations of the transmembrane-cytoplasmic domains of integrin α IIb β 3 show that the IMC is loosened with the presence of talin, most likely through membrane-proximal interactions which result from the energetic compensation of the weakened IMC by K320 on the S1-S2 loop of talin. We also found, using the full-length crystal structure we built, that talin has a larger role in integrin activation by disrupting a new stable clasp (R734-E1006) through the initial membrane-distal interactions that anchors talin to integrin (2). Furthermore, we used this full-length crystal structure of integrin α IIb β 3 to explore binding sites

of soluble RGD ligands and their potent to activate integrin α I**II** β 3 or maintain it in the activated state. We found three major groups of bindings with two specific binding sites corresponding to each group. According to our simulations, the major group of interactions that maintains integrin α I**II** β 3 in the inactive, bent state occurs between Lys350 on β A domain, and Ser673 and Ser674 on the β TD. Interestingly, we observed full dissociation of β TD and β A domains when this interaction group was disrupted and eventually removed as a result of a competition between Arg of the RGD peptide with Ser674. Therefore, we proposed this molecular scenario as a potential triggering mechanism for outside-in activation of integrin α I**II** β 3 by soluble RGD ligand.

References

1. Lau TL, Kim C, Ginsberg MH, Ulmer TS. 2009. The structure of the integrin alphaIIb beta3 transmembrane complex explains integrin transmembrane signalling. *EMBO J* 28: 1351-61
2. Anthis NJ, Campbell ID. 2011. The tail of integrin activation. *Trends Biochem Sci* 36: 191-8
3. Barczyk M, Carracedo S, Gullberg D. 2010. Integrins. *Cell Tissue Res* 339: 269-80
4. Shattil SJ, Kim C, Ginsberg MH. 2010. The final steps of integrin activation: the end game. *Nat Rev Mol Cell Biol* 11: 288-300
5. Jones ML, Harper MT, Aitken EW, Williams CM, Poole AW. 2010. RGD-ligand mimetic antagonists of integrin alphaIIb beta3 paradoxically enhance GPVI-induced human platelet activation. *J Thromb Haemost* 8: 567-76
6. Ma YQ, Qin J, Plow EF. 2007. Platelet integrin alpha(IIb)beta(3): activation mechanisms. *J Thromb Haemost* 5: 1345-52
7. Shattil SJ, Newman PJ. 2004. Integrins: dynamic scaffolds for adhesion and signaling in platelets. *Blood* 104: 1606-15
8. Zou Z, Chen H, Schmaier AA, Hynes RO, Kahn ML. 2007. Structure-function analysis reveals discrete beta3 integrin inside-out and outside-in signaling pathways in platelets. *Blood* 109: 3284-90
9. Vinogradova O, Velyvis A, Velyviene A, Hu B, Haas T, Plow E, Qin J. 2002. A structural mechanism of integrin alpha(IIb)beta(3) "inside-out" activation as regulated by its cytoplasmic face. *Cell* 110: 587-97
10. Xiao T, Takagi J, Collier BS, Wang JH, Springer TA. 2004. Structural basis for allostery in integrins and binding to fibrinogen-mimetic therapeutics. *Nature* 432: 59-67
11. Xiong JP, Stehle T, Diefenbach B, Zhang R, Dunker R, Scott DL, Joachimiak A, Goodman SL, Arnaout MA. 2001. Crystal structure of the extracellular segment of integrin alpha Vbeta3. *Science* 294: 339-45
12. Xiong JP, Stehle T, Zhang R, Joachimiak A, Frech M, Goodman SL, Arnaout MA. 2002. Crystal structure of the extracellular segment of integrin alpha Vbeta3 in complex with an Arg-Gly-Asp ligand. *Science* 296: 151-5
13. Springer TA, Zhu J, Xiao T. 2008. Structural basis for distinctive recognition of fibrinogen gammaC peptide by the platelet integrin alphaIIb beta3. *J Cell Biol* 182: 791-800
14. Takagi J, Petre BM, Walz T, Springer TA. 2002. Global conformational rearrangements in integrin extracellular domains in outside-in and inside-out signaling. *Cell* 110: 599-11
15. D'Souza SE, Haas TA, Piotrowicz RS, Byers-Ward V, McGrath DE, Soule HR, Cierniewski C, Plow EF, Smith JW. 1994. Ligand and cation binding are dual functions of a discrete segment of the integrin beta 3 subunit: cation displacement is involved in ligand binding. *Cell* 79: 659-67
16. Plow EF, Haas TA, Zhang L, Loftus J, Smith JW. 2000. Ligand binding to integrins. *J Biol Chem* 275: 21785-8
17. Friedland JC, Lee MH, Boettiger D. 2009. Mechanically activated integrin switch controls alpha5beta1 function. *Science* 323: 642-4
18. Kong F, Garcia AJ, Mould AP, Humphries MJ, Zhu C. 2009. Demonstration of catch bonds between an integrin and its ligand. *J Cell Biol* 185: 1275-84

19. Zhu J, Boylan B, Luo BH, Newman PJ, Springer TA. 2007. Tests of the extension and deadbolt models of integrin activation. *J Biol Chem* 282: 11914-20
20. Xiong JP, Stehle T, Goodman SL, Arnaout MA. 2003. New insights into the structural basis of integrin activation. *Blood* 102: 1155-9
21. Beglova N, Blacklow SC, Takagi J, Springer TA. 2002. Cysteine-rich module structure reveals a fulcrum for integrin rearrangement upon activation. *Nat Struct Biol* 9: 282-7
22. Jin M, Andricioaei I, Springer TA. 2004. Conversion between three conformational states of integrin I domains with a C-terminal pull spring studied with molecular dynamics. *Structure* 12: 2137-47
23. Chen W, Lou J, Hsin J, Schulten K, Harvey SC, Zhu C. 2011. Molecular Dynamics Simulations of Forced Unbending of Integrin alpha(V)beta(3). *PLoS Comput Biol* 7: e1001086
24. Arnaout MA, Mahalingam B, Xiong JP. 2005. Integrin structure, allostery, and bidirectional signaling. *Annu Rev Cell Dev Biol* 21: 381-410
25. Phillips JC, Braun R, Wang W, Gumbart J, Tajkhorshid E, Villa E, Chipot C, Skeel RD, Kale L, Schulten K. 2005. Scalable molecular dynamics with NAMD. *J Comput Chem* 26: 1781-802
26. Zhu J, Luo BH, Xiao T, Zhang C, Nishida N, Springer TA. 2008. Structure of a complete integrin ectodomain in a physiologic resting state and activation and deactivation by applied forces. *Mol Cell* 32: 849-61
27. Humphrey W, Dalke A, Schulten K. 1996. VMD: visual molecular dynamics. *J Mol Graph* 14: 33-8, 27-8
28. Lodish HF. 2008. *Molecular cell biology*. New York: W.H. Freeman. 1 v. (various pagings) pp.
29. Krautler V, Van Gunsteren WF, Hunenberger PH. 2001. A fast SHAKE: Algorithm to solve distance constraint equations for small molecules in molecular dynamics simulations. *Journal of Computational Chemistry* 22: 501-8
30. Wegener KL, Partridge AW, Han J, Pickford AR, Liddington RC, Ginsberg MH, Campbell ID. 2007. Structural basis of integrin activation by talin. *Cell* 128: 171-82
31. Tadokoro S, Shattil SJ, Eto K, Tai V, Liddington RC, de Pereda JM, Ginsberg MH, Calderwood DA. 2003. Talin binding to integrin beta tails: a final common step in integrin activation. *Science* 302: 103-6
32. Yang J, Ma YQ, Page RC, Misra S, Plow EF, Qin J. 2009. Structure of an integrin alphaIIb beta3 transmembrane-cytoplasmic heterocomplex provides insight into integrin activation. *Proc Natl Acad Sci U S A* 106: 17729-34
33. Elliott PR, Goult BT, Kopp PM, Bate N, Grossmann JG, Roberts GC, Critchley DR, Barsukov IL. 2010. The Structure of the talin head reveals a novel extended conformation of the FERM domain. *Structure* 18: 1289-99
34. Anslyn EV, Dougherty DA. 2006. *Modern physical organic chemistry*. Sausalito, Calif.: University Science. xxviii, 1099 p. pp.
35. Kollman JM, Pandi L, Sawaya MR, Riley M, Doolittle RF. 2009. Crystal structure of human fibrinogen. *Biochemistry* 48: 3877-86
36. Kumar S, Nussinov R. 2002. Close-range electrostatic interactions in proteins. *Chembiochem* 3: 604-17

37. Garcia-Alvarez B, de Pereda JM, Calderwood DA, Ulmer TS, Critchley D, Campbell ID, Ginsberg MH, Liddington RC. 2003. Structural determinants of integrin recognition by talin. *Mol Cell* 11: 49-58
38. Furie B, Furie BC. 2008. Mechanisms of thrombus formation. *N Engl J Med* 359: 938-49
39. Leng LJ, Kashiwagi H, Ren XD, Shattil SJ. 1998. RhoA and the function of platelet integrin alpha(IIb)beta(3). *Blood* 91: 4206-15
40. Parise LV. 1999. Integrin alpha(IIb)beta(3) signaling in platelet adhesion and aggregation. *Current Opinion in Cell Biology* 11: 597-601
41. Shattil SJ, Kashiwagi H, Pampori N. 1998. Integrin signaling: The platelet paradigm. *Blood* 91: 2645-57
42. Adair BD, Yeager M. 2002. Three-dimensional model of the human platelet integrin alpha IIbbeta 3 based on electron cryomicroscopy and x-ray crystallography. *Proc Natl Acad Sci U S A* 99: 14059-64
43. Askari JA, Buckley PA, Mould AP, Humphries MJ. 2009. Linking integrin conformation to function. *J Cell Sci* 122: 165-70
44. Hantgan RR, Paumi C, Rocco M, Weisel JW. 1999. Effects of ligand-mimetic peptides Arg-Gly-Asp-X (X = Phe, Trp, Ser) on alphaIIbbeta3 integrin conformation and oligomerization. *Biochemistry* 38: 14461-74
45. Loftus JC, Liddington RC. 1997. Cell adhesion in vascular biology. New insights into integrin-ligand interaction. *J Clin Invest* 99: 2302-6
46. Boyce SE, Mobley DL, Rocklin GJ, Graves AP, Dill KA, Shoichet BK. 2009. Predicting ligand binding affinity with alchemical free energy methods in a polar model binding site. *J Mol Biol* 394: 747-63
47. Carey VP. 1999. *Statistical thermodynamics and microscale thermophysics*. Cambridge, UK ; New York: Cambridge University Press. xvii, 414 p. pp.
48. Kamata T, Tieu KK, Irie A, Springer TA, Takada Y. 2001. Amino acid residues in the alpha IIb subunit that are critical for ligand binding to integrin alpha IIbbeta 3 are clustered in the beta-propeller model. *J Biol Chem* 276: 44275-83
49. Takagi J, Erickson HP, Springer TA. 2001. C-terminal opening mimics 'inside-out' activation of integrin alpha5beta1. *Nat Struct Biol* 8: 412-6
50. Calzada MJ, Alvarez MV, Gonzalez-Rodriguez J. 2002. Agonist-specific structural rearrangements of integrin alpha IIbbeta 3. Confirmation of the bent conformation in platelets at rest and after activation. *J Biol Chem* 277: 39899-908
51. Cierniewski CS, Byzova T, Papierak M, Haas TA, Niewiarowska J, Zhang L, Cieslak M, Plow EF. 1999. Peptide ligands can bind to distinct sites in integrin alphaIIbbeta3 and elicit different functional responses. *J Biol Chem* 274: 16923-32
52. Gottschalk KE, Adams PD, Brunger AT, Kessler H. 2002. Transmembrane signal transduction of the alpha(IIb)beta(3) integrin. *Protein Sci* 11: 1800-12
53. Kim M, Carman CV, Springer TA. 2003. Bidirectional transmembrane signaling by cytoplasmic domain separation in integrins. *Science* 301: 1720-5

Tables

	β -Propeller of α -Subunit	β A of β -Subunit
RGD1	Glu48	Pro166
RGD2	Ser46, Gln47, Glu48, Arg153, Glu157	Pro166
RGD3	Asp805, Asn309, Asp628, Lys590, Arg851	Asp123, Glu308, Lys640, Asp232, Asp661, Lys590, Lys601

Table 1: Several binding sites for RGD peptides on integrin were found. Most binding sites were near the β A- β TD pocket.

	cyto- β 3	NPLY	W739-NPLY	A710-NPLY	NPLY-T762
1. Interaction Energy	-0.81, 0.0049**	-0.62, 0.0537	-0.77, 0.0092**	-0.45, 0.1869	-0.82, 0.0038**
2. R734-E1006 Distance	-0.70, 0.0251*	-0.54, 0.1076	-0.67, 0.0330*	-0.26, 0.4671	-0.65, 0.0425*

Table 2: Correlational values (presented in the format of “rho, p-value”) using Spearman’s rho of the distance between the centers of mass with selected regions of integrin β 3-subunit and talin-1 F3 domain to: (1) the energy of interaction between R734-E1006; (2) the distance between most terminal carbons on R734 and E1006. This table shows that using energy of interaction to quantify the extra interaction of R734-E1006 produces a more stable and significant result than does distance. A comparison of these correlational values suggests that talin binding to the membrane distal region of β 3-tail (NPLY-T762) is most important in weakening the extra interaction. (* = $p < 0.05$, ** = $p < 0.01$).

	1. α IIB- β 3 extracellular domains	2. β TD- β A domains
Centers of Mass Distance	-0.12, 0.75	-0.26, 0.47
VdW	0.41, 0.24	0.26, 0.47
Interaction energy Electrostatic	0.05, 0.88	-0.21, 0.56
Total Non-bond	0.05, 0.88	-0.27, 0.45

Table 3: Correlational values (presented in the format of “rho, p-value”) using Spearman’s rho of the distance between the center of mass with the cytoplasmic domain of integrin β 3-subunit and talin-1 F3 domain to the center of mass distance or interaction energies of (1) α IIB and β 3 extracellular domains and (2) β TD and β A domains. This table shows that there are no significant changes to the extracellular domains of integrin with relation to talin binding to integrin.

Legends

Figure 1: A schematic of one of the main pathways of integrin α IIB β 3 inside-out activation. Binding of thrombin to proteinase-activated receptor 1 (PAR1) causes separation of talin head and tail domains. Consequently, talin head domain associates with β 3-subunit cytoplasmic domain, activating integrin α IIB β 3.

Figure 2: Crystal structure of integrin α IIB β 3 embedded in the plasma membrane. Three RGD peptides (green) are positioned in potential binding regions of integrin. The only RGD sequence that interacted with the integrin molecule was the one located near β TD- β A pocket (RGD3). α IIB- and β 3-subunits are depicted in red and blue, respectively. The plasma membrane is shown in gold.

Figure 3: Distance between interacting residues of integrin with the RGD peptide for RGD-included runs. (a) and (b) represent the type1 interaction with only a permanent bond between Arg of the RGD peptide and integrin. (c) and (d) are corresponding to type2 interactions, wherein Arg of the RGD interacts permanently with integrin while Asp of the RGD peptide interacts only temporarily with another single residue of integrin. (e) and (f) show the cases where Arg of RGD permanently bound to a residue of integrin and the side chain of Asp of the RGD switched back and forth between two other residues of integrin, which is called type3 binding.

Figure 4: Arg of RGD disrupts the β A- β TD interactions via competing with K350 on β A domain for S673. (a) β A and β TD domains are attached in the inactive, bent state of integrin. (b) The β TD swings open and separates apart from β A domain, which leads to integrin activation. (c) Focusing further into the β TD- β A pocket shows the key interaction between K350 and S673/S674 that keeps integrin inactive. (d) The RGD peptide approaches S674 and interacts with it, disrupting the key interaction between β TD and β A domains. (e) While Arg of the RGD peptide is bound to E671 and S674, Asp of the RGD peptide switches back and forth between K600 and K611. This competitive interaction on the Asp side of the RGD peptide shifts the β TD further toward EGF3/4 domains and apart from β A domain.

Figure 5: (a) Interaction energy between integrin transmembrane-cytoplasmic domains of α - and β -subunits as the simulation progresses for the integrin activation case as well as for the simulation with no RGD peptide. The initial 5ns of the simulation demonstrates the pre-equilibration phase, where both systems show similar interaction energies of \sim 250 kCal/mol. This energy finally reaches a stable state at \sim 200kCal/mol in the absence of an RGD peptide. However, for the case where separation between integrin β TD and β A domains occurs, the energy of interaction between the transmembrane-cytoplasmic domains of integrin is significantly drops to \sim 100 kCal/mol. This difference highlights a potential underlying mechanism that could loosen and eventually break apart the electrostatic interaction that holds the transmembrane-cytoplasmic domains of integrin together, as a result of an RGD-induced outside-in activation. (b) A schematic of integrin α IIB β 3 immediately after activation via RGD binding to the β TD. Integrin β TD and β A domains are bound by the key interaction group. Insertion of an RGD peptide into the β TD- β A pocket leads to a separation between β TD and β A domains that somehow unbends integrin, while loosens the electrostatic interaction between integrin transmembrane domains via rotating the transmembrane domain of β -subunit.

Figure 6: (a) Initial simulation position of integrin α IIB β 3 transmembrane-cytoplasmic domains (PDB 2K9J) and Talin-1 FERM domain (PDB 3IVF). For the new-cartoon representations, in red is α IIB-subunit of integrin, in blue is β 3-subunit of integrin, and in silver is talin-1 FERM domain. For van der Waals sphere representations, in orange are the acidic residues E1006 (on α IIB) and D723 (on β 3) integrin, in cyan are the basic residues and R734 (on β 3), in green are the residues F727, F730, and W739 (from top going down on β 3), in pink is the NPLY motif, in brown are residues R358, A360, A389, Q390, A393, and I398 on talin F3 domain, and in yellow is K320 of the S1-S2 loop on talin-1 F3 domain. Note that the CPK representation in cyan (R995, α IIB) and orange (E726, β 3) are tightly bound to hold the IMC together. These highlighted residues play an important role as discussed in literature and is shown by our simulations. (b + c) Talin-1 F3 domain (F0-F2 not shown) binding with NPLY motif and W739 on integrin β 3 subunit. The left rendering (b) highlights NPLY motif binding to H1 helix; while the right rendering (c) highlights W739 binding in the pocket formed by R358 and A360 in talin. Time taken is at 24ns after the start of the simulation.

Figure 7: (a, b) Total nonbonding (van der Waals and electrostatic) energy between the IMC residues - R995 on α IIB- and D723 and E726 on β 3-subunits – for the steered molecular dynamics simulations, where α IIB R995 carbon- α atom was pulled ($k = 0.05\text{kcal/mol/\AA}^2$, velocity = 10\AA/ns) and the β 3 D723 and E726 carbon- α atoms were fixed. The colored lines represent the raw data from each of the 12 trials per condition, whereas the dark black line indicates the average of these trials. The two vertical dark gray bars within the first 100ps indicate the averaged region to obtain the initial nonbonding energy prior to performing SMD. The graph on the left (a) is the integrin-alone condition, while the right (b) is with talin bound to integrin. (c) Work done by the SMD simulations to separate the IMC by the amount of distance between the carbon- α atoms.

Figure S1: Disruption of the key interaction group K350-S673/674 detaches β TD and β A domains. (a) Distance between S673 and K350 as a function of the simulation time for six RGD-included as well as one non-RGD run (light blue). The simulation that led to β A- β TD detachment is shown in purple. The interaction is disrupted at \sim 7.5ns (b) Distance between S674 and K350 as a

function of the simulation time for six RGD-included as well as one non-RGD run (light blue). The simulation that led to β A- β TD detachment is shown in purple.

Figure S2: Tan atom 2.0x magnification is pulled atom, two purple atoms 2.0x magnification are the fixed atoms. This is the same for integrin-talin or integrin-only systems. Distance “d” is the distance measured between the IMC residues.

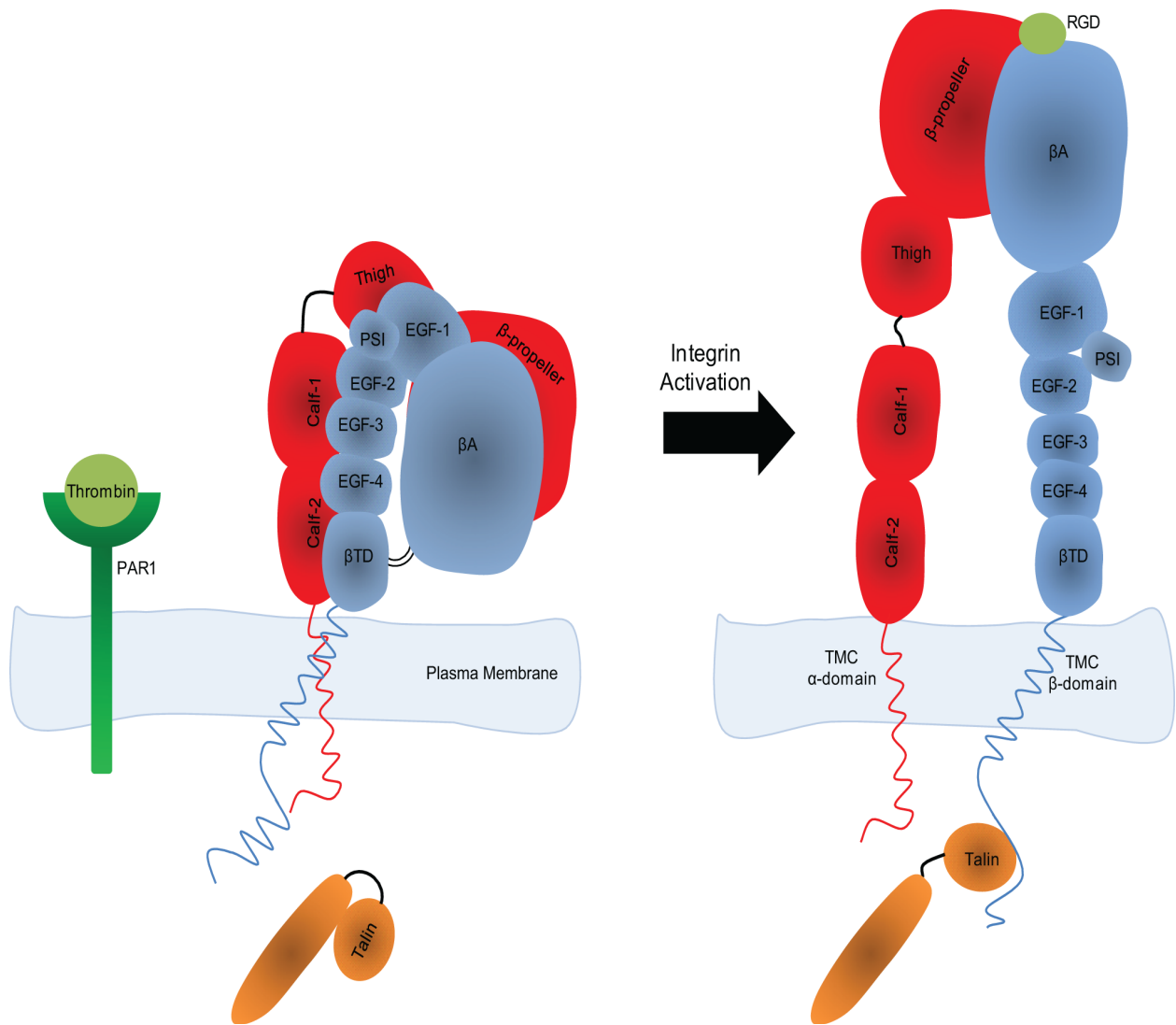


Figure 1

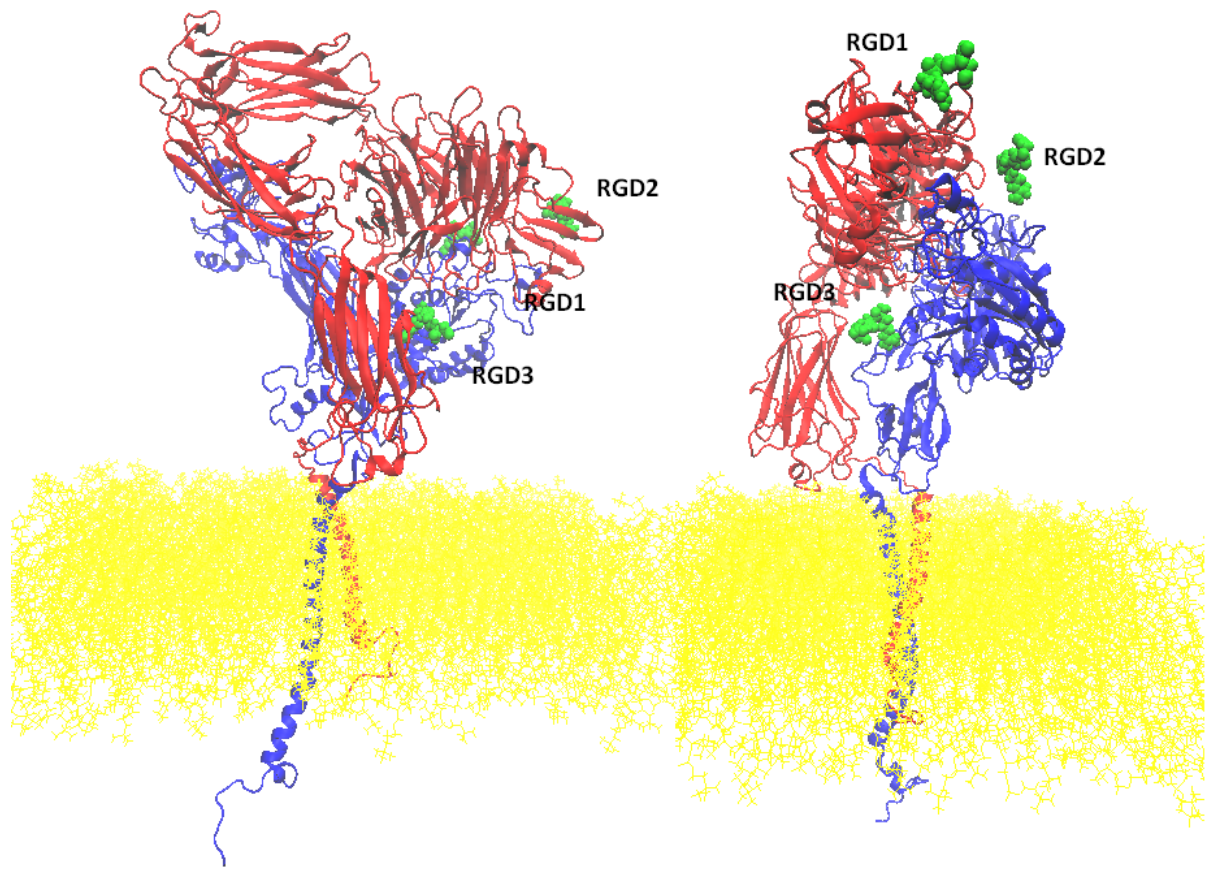
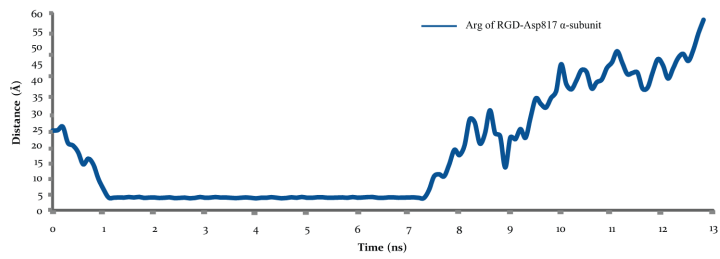
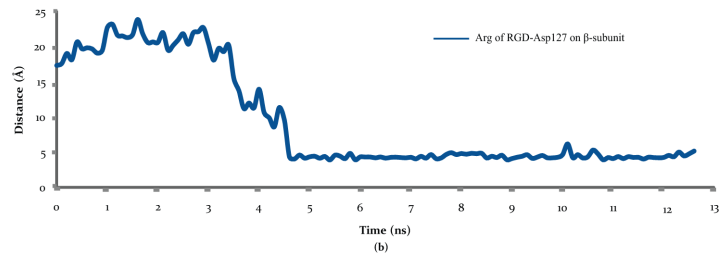


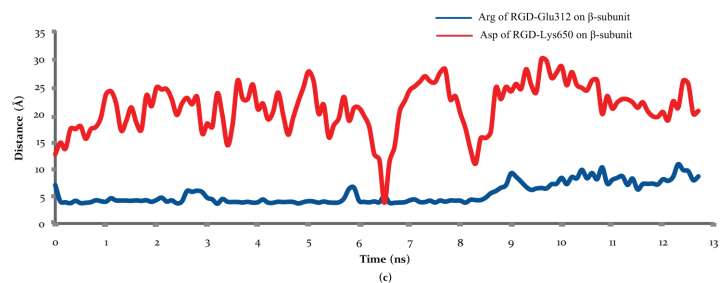
Figure 2



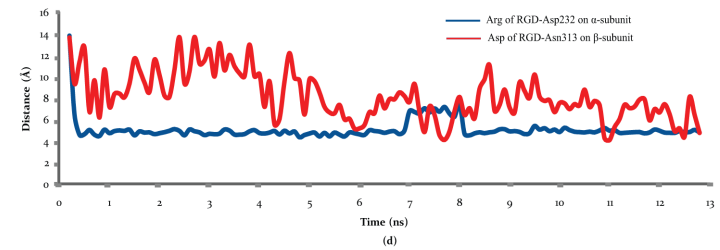
(a)



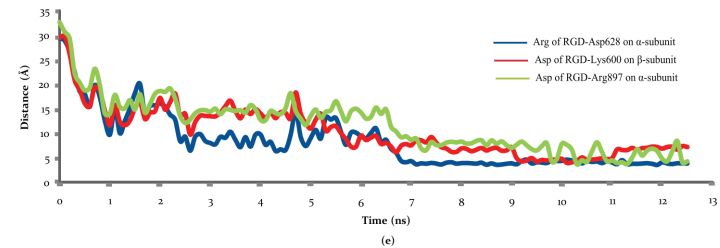
(b)



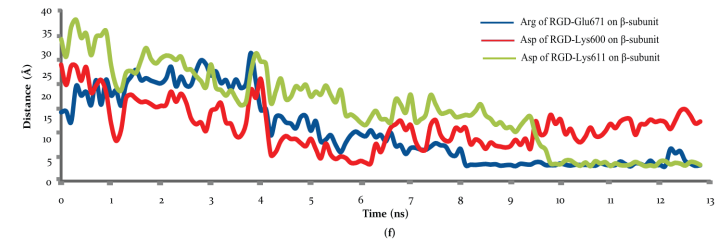
(c)



(d)



(e)



(f)

Figure 3

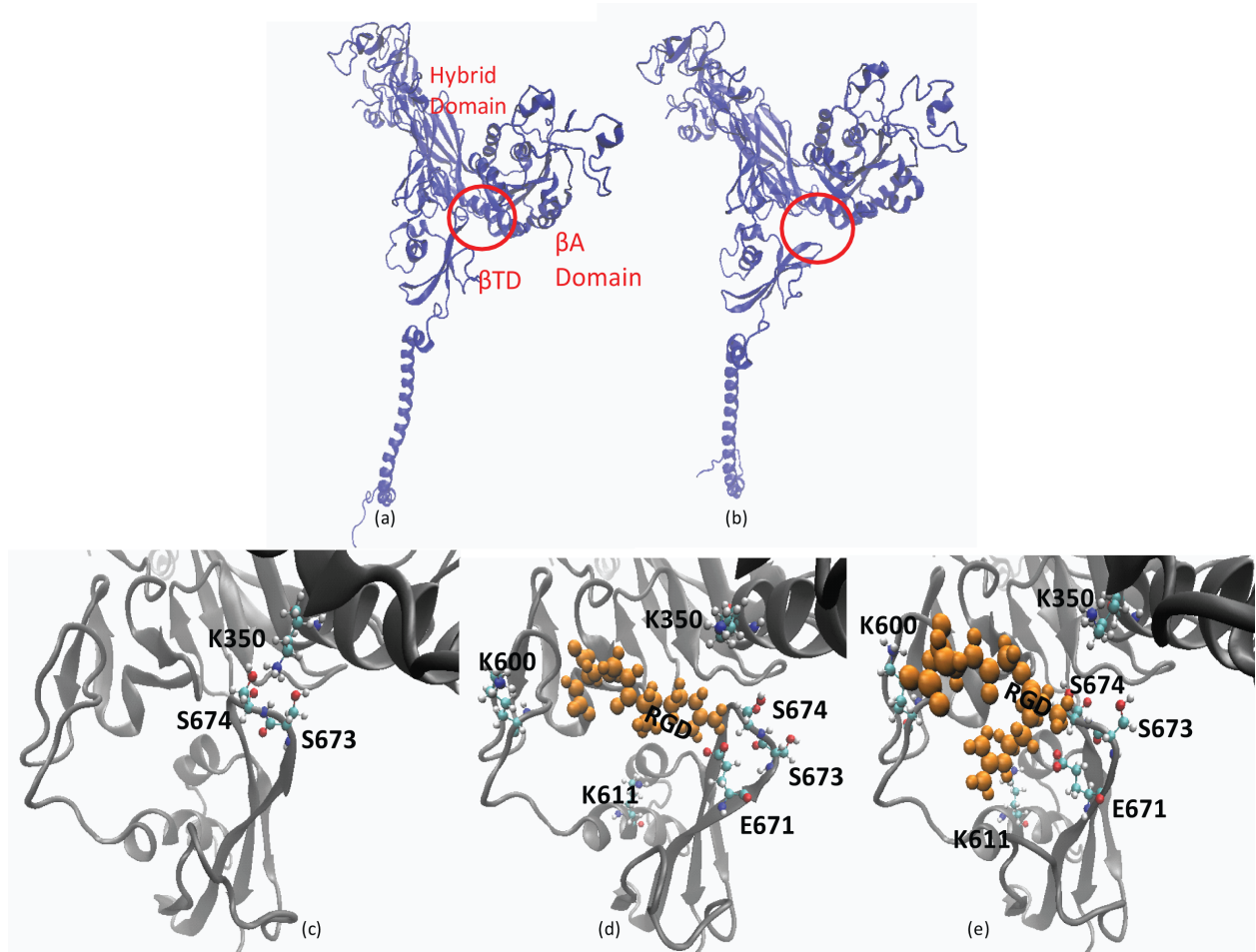
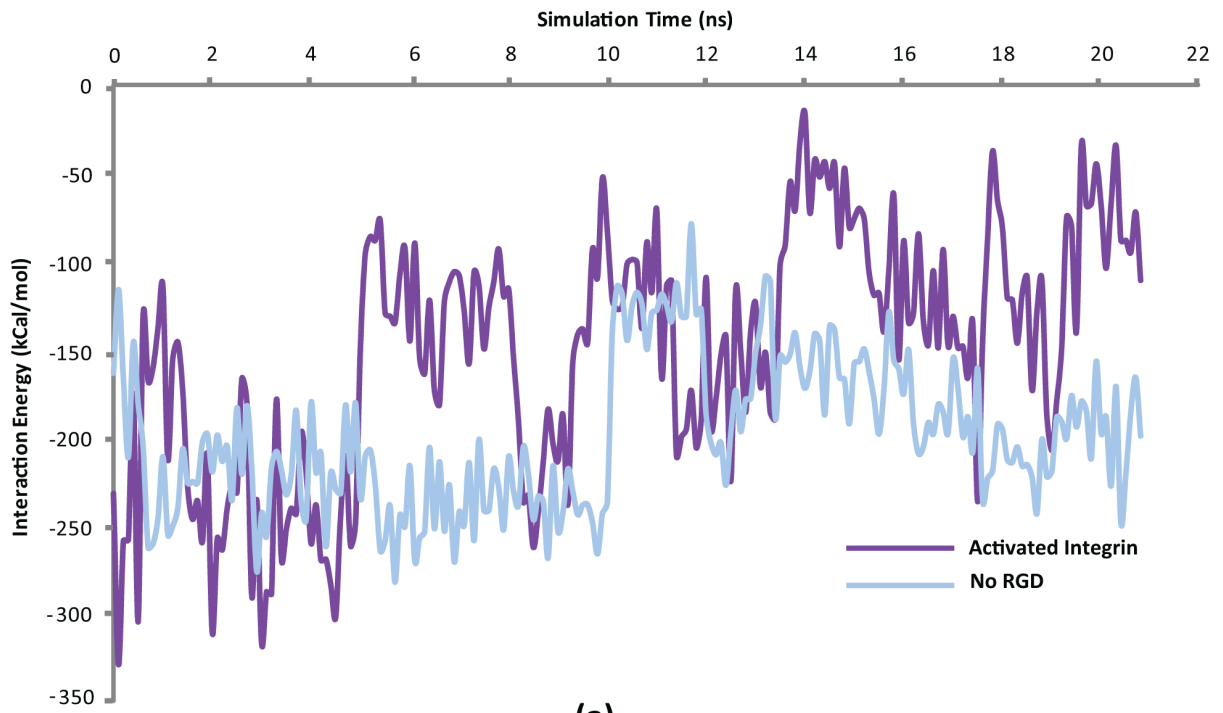
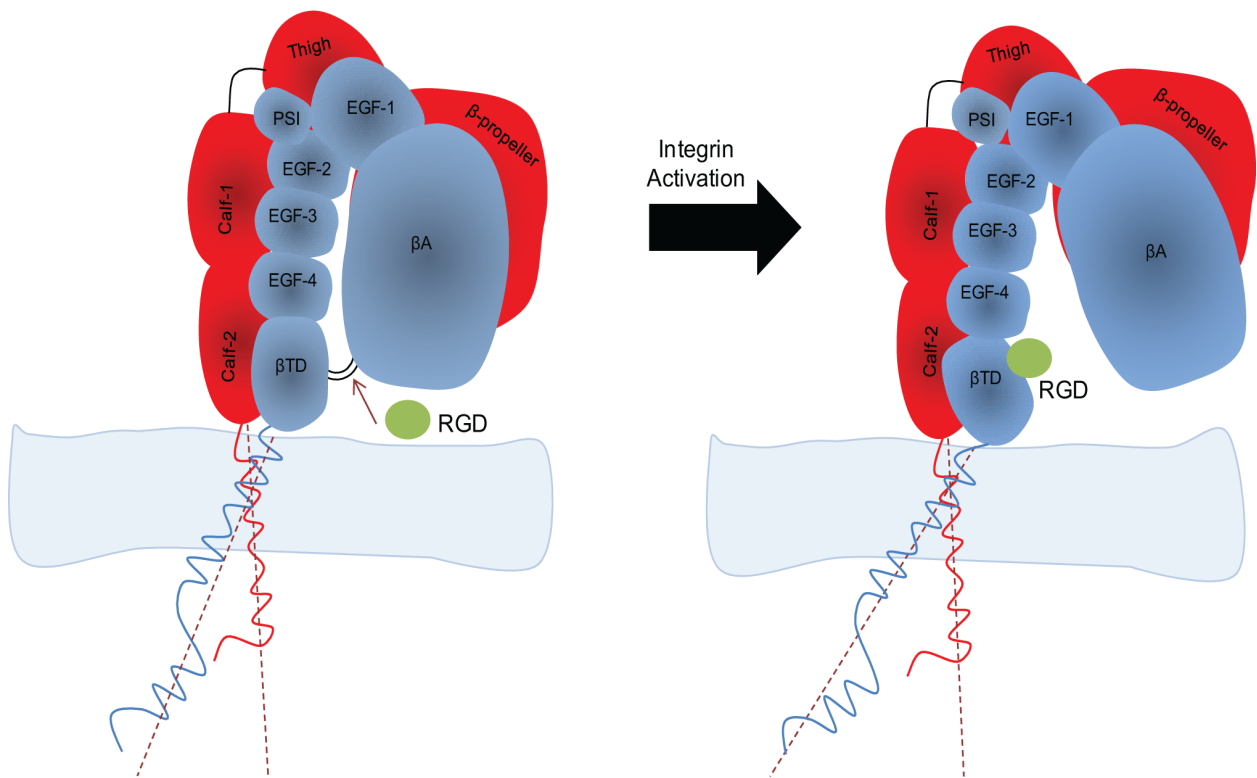


Figure 4



(a)



(b)

Figure 5

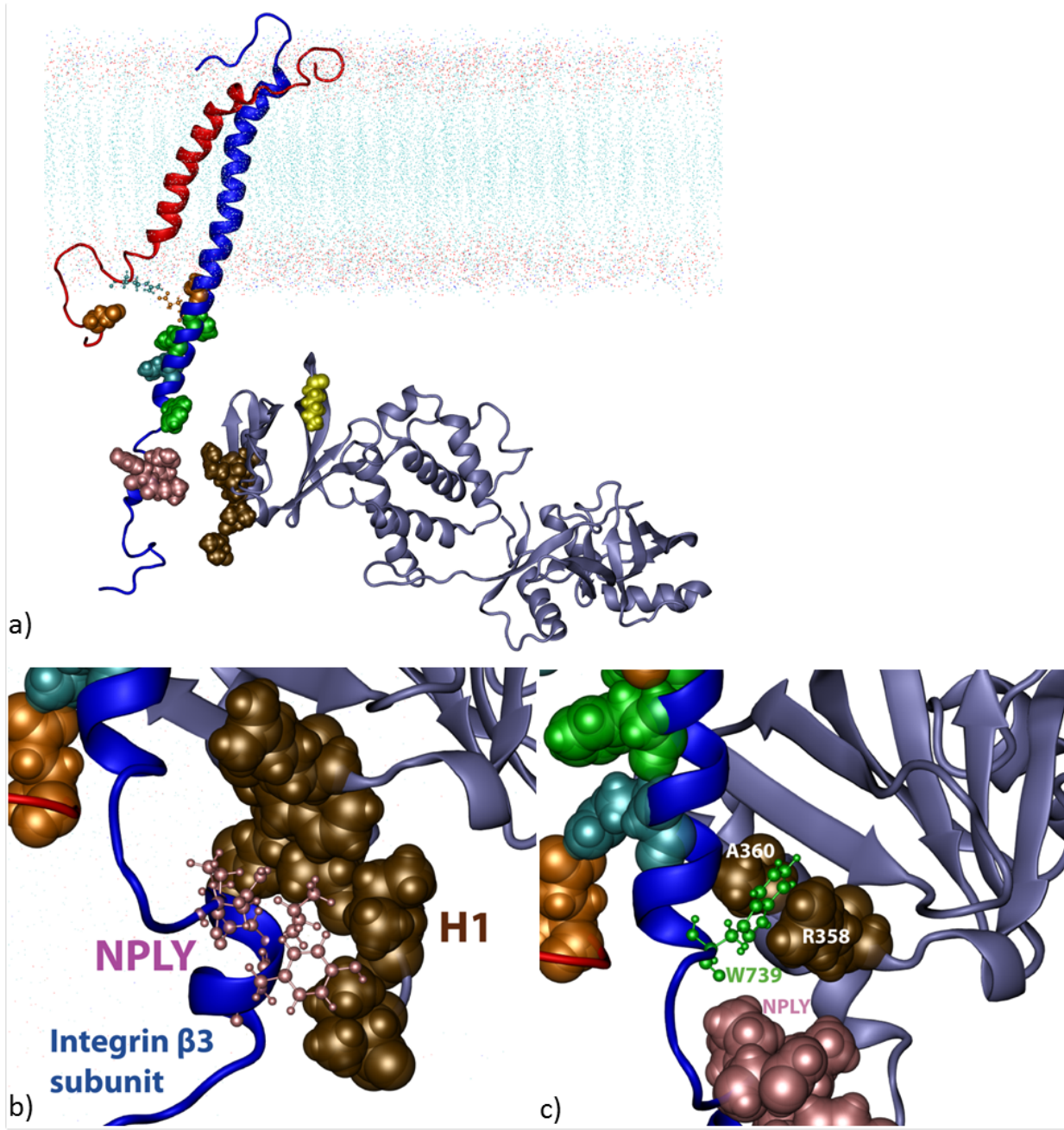


Figure 6

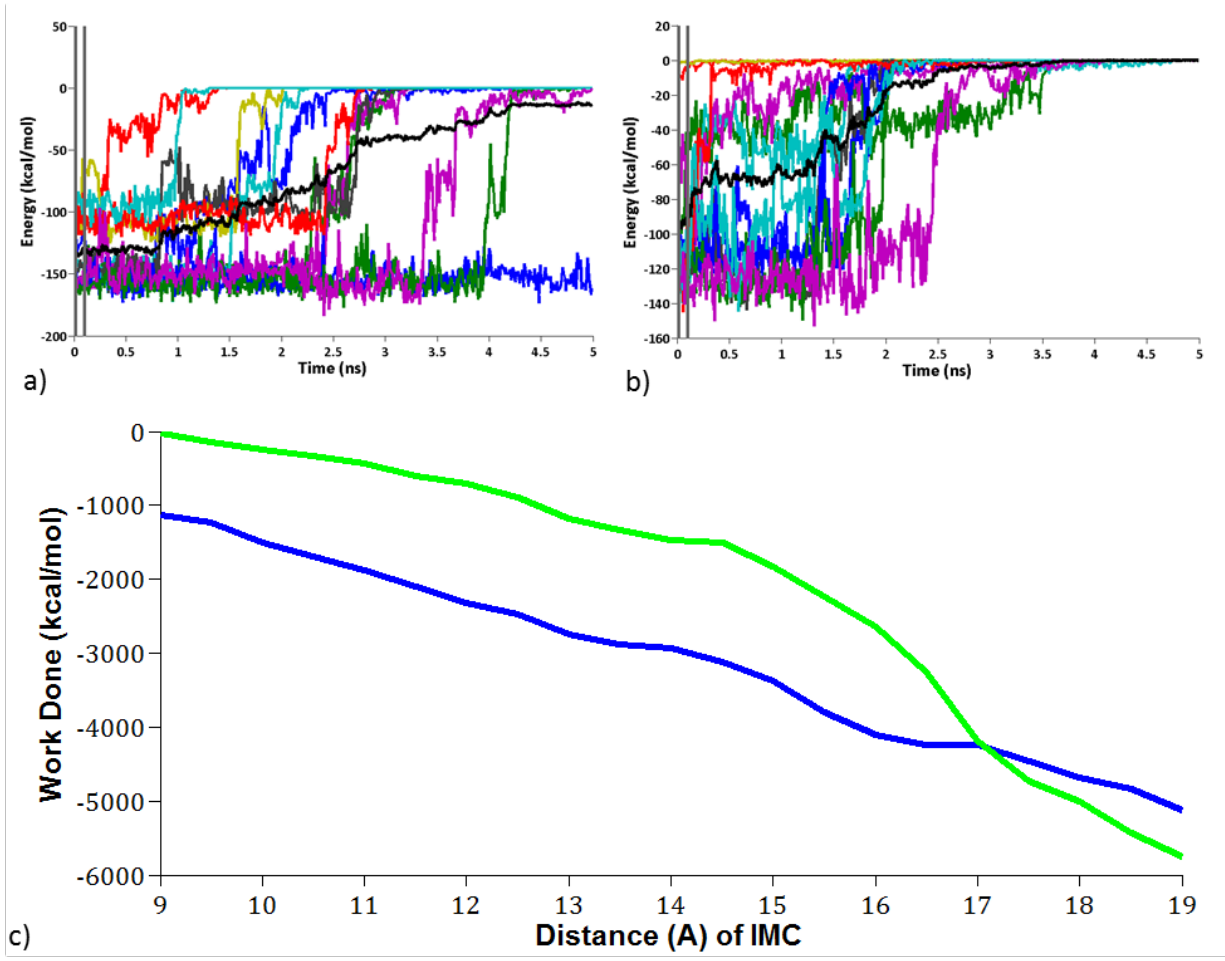
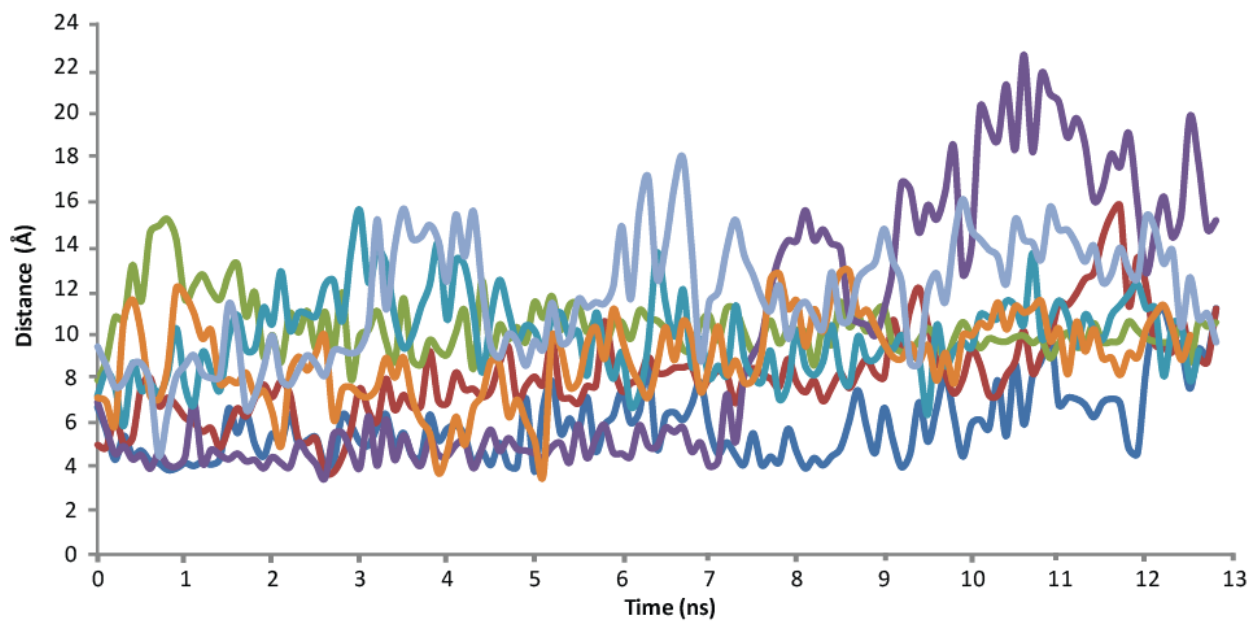
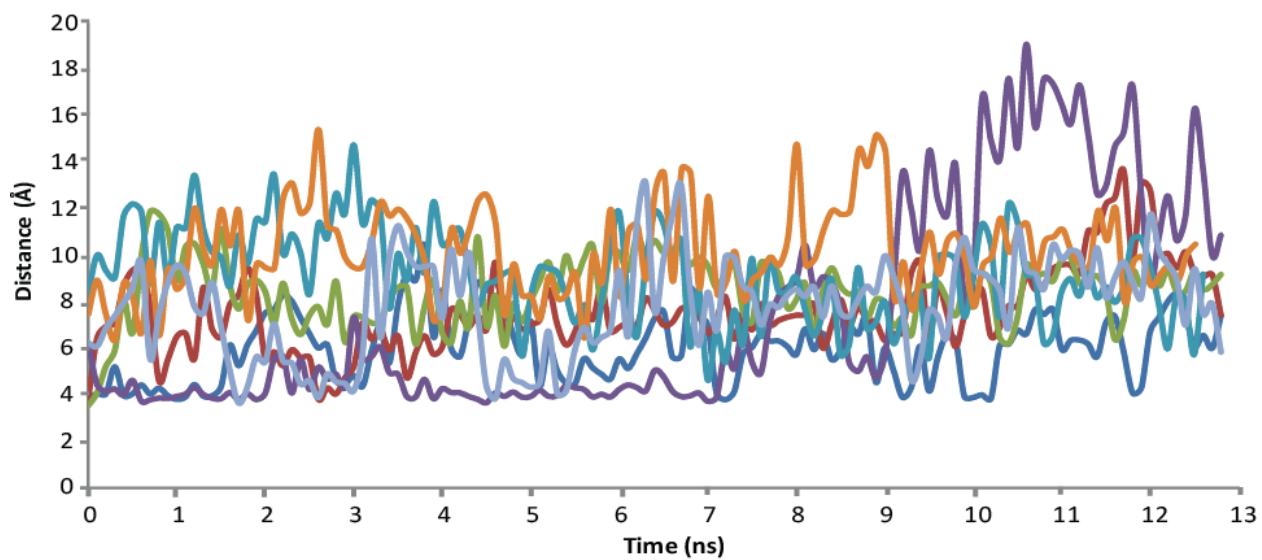


Figure 7



(a)



(b)

Figure S1

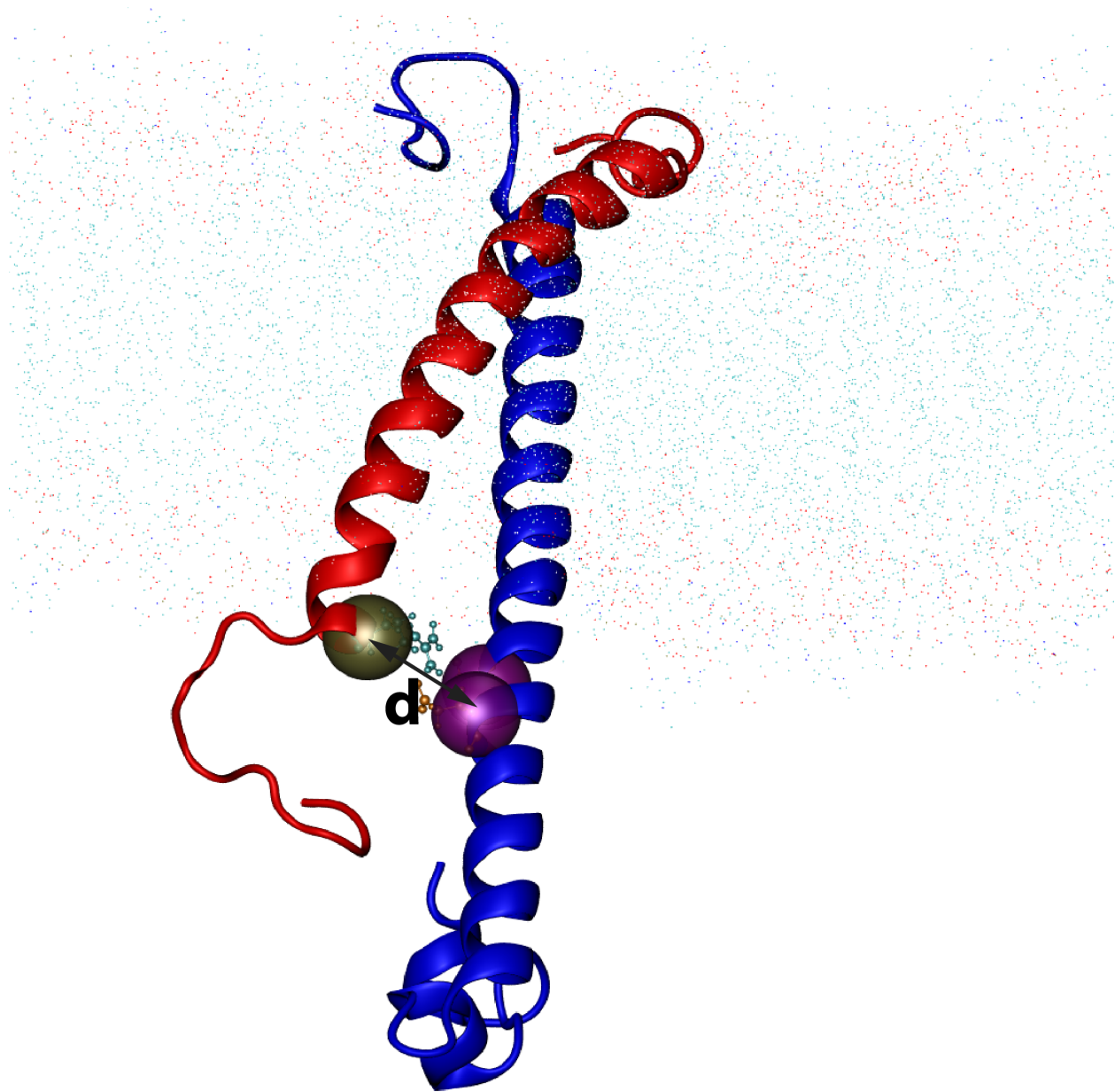


Figure S2